Design of a hybrid powertrain consisting of battery and fuel cell

Dr Armin U. Schmiegel, REFU Drive GmbH, University of Applied Science, Reutlingen

1. Introduction

Climate change and rising energy prices, as well as the continuous improvement of power electronic components, storage and drive technology, are driving the change towards the electrification of mobile machines [1][2][3]. In some cases, the requirements for mobile machines are different from those for passenger vehicles. Commercial vehicles, for example, are usually used permanently over a longer period of time, whereas passenger vehicles are mostly stationary. Likewise, the load profiles for mobile machinery have a different structure, as commercial vehicles require higher power over a longer period of time. At the same time, the load profiles show greater fluctuations.

As an example of the complexity of the design, in [4] we dealt with the question of how high the power of a generator or battery must be selected for a straddle carrier. Three possible technical implementations of the powertrain, diesel-electric, hybrid and all-electric, were each individually optimised.

In this whitepaper, we will now look at a different system. A long-haul transporter equipped with a fuel cell and a lithium-ion battery. The use of fuel cells as the main energy source was considered in [2] for different system topologies. Comparable to the work in [4] and [5] the load profile of a straddle carrier was considered here. The focus of the considerations was the design of the fuel cell hybrid powertrains with regard to their performance. In [6] a hybrid-powered tram was considered. When combining different energy sources, it is necessary to define an operating strategy. The chosen approaches range from the use of model predictive approaches and fuzzy control to global optimisation strategies and state machine based control [7]. Since the strategy also always influences the design, an approach that is independent of the technical implementation would make sense here. Already in [8]-[11] it could be shown that the system description by power flow diagrams with the resulting simple optimisation task is an approach to combine the question of the optimal strategy with the question of an optimal design. In this approach, the choice of strategy is made based on an optimisation criterion that analyses the yield or the losses. If this problem is used with full knowledge of the production and load profiles, it is possible to identify a globally optimal strategy, which thus describes the best possible realisation.

2. The hybrid-powered drivetrain

In Figure 2-1 the hybrid powertrain is shown. The electric drive is connected to a DC bus to which a battery and a fuel cell are connected. Since the voltage levels of the battery and the fuel cell are different, both are connected to the DC bus via a DC/DC controller.

Alternatively, a topology could be chosen here in which the battery voltage determines the voltage of the DC bus.

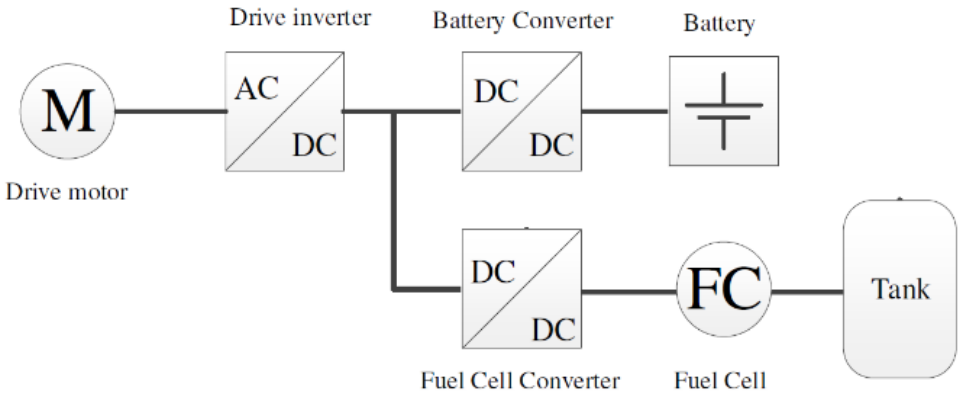

Figure 2-1 : Schematic representation of a hybrid powertrain consisting of battery and fuel cell.

For the design of this system, the question arises how much energy should be stored in the battery and in the fuel cell. The battery has the advantage that it can be charged both by the fuel cell and by recuperation. The fuel cell, on the other hand, has the advantage that the amount of energy available is determined by the size of the hydrogen tank and this can be scaled. The charging times for a hydrogen tank are - compared to the battery - significantly shorter.

Unlike lithium-ion batteries, fuel cells are not able to respond to high or rapid power fluctuations [12]. The reason is that an equilibrium between reactants and charge carriers is required for the operation of a fuel cell at the membrane. This equilibrium is disturbed in the case of strong or rapid power fluctuations [8]. This can lead to an excess of water (flooding) or an undersupply of hydrogen (dehydration). This effect is all the stronger the more stacks flow in series [13].

If there is too much water in the stack, no exchange can take place across the membrane wall, as hydrogen and oxygen can no longer react through the membrane. If hydrogen is missing, the reaction rate is reduced, which leads to an increased polarisation that damages the membrane, as the oxygen now reacts with the material of the membrane.

A suitable strategy is to continuously charge the battery with the fuel cell so that the discharge power of the fuel cell is not subject to strong fluctuations od the driving profile and there is always enough energy in the battery.

3. Description of the hybrid powertrain with the aid of the power flow diagram

To analyse the influence of the various parameters on the performance of the overall system, we use a system description of the vehicle in the power flow diagram.
In this representation, the various components are abstracted to power sources, storage and sinks. Power can be transferred between these power nodes. The technological boundary conditions of different realisations are then described by the efficiency and restrictions in the power transport.

In Figure 3-1 the power flow diagram of the vehicle is shown. It consists of two storage nodes, the fuel cell F and the battery Bwhich supply the load L supply. We describe the storage process by transferring power into the future at time $t + \Delta$ or receiving power from the past at the point in time $t - \Delta$ time.

Here we work with a discrete-time description with a time increment Δ. Both storage nodes can therefore obtain power from the past or transfer it to a node in the future. $B(-\Delta), F(-\Delta)$ or transfer power to a node in the future $B(\Delta), F(\Delta)$. The power demand of the vehicle is mapped via a load profile $\tilde{L}$ which defines for each point in time how much power the drive requires.

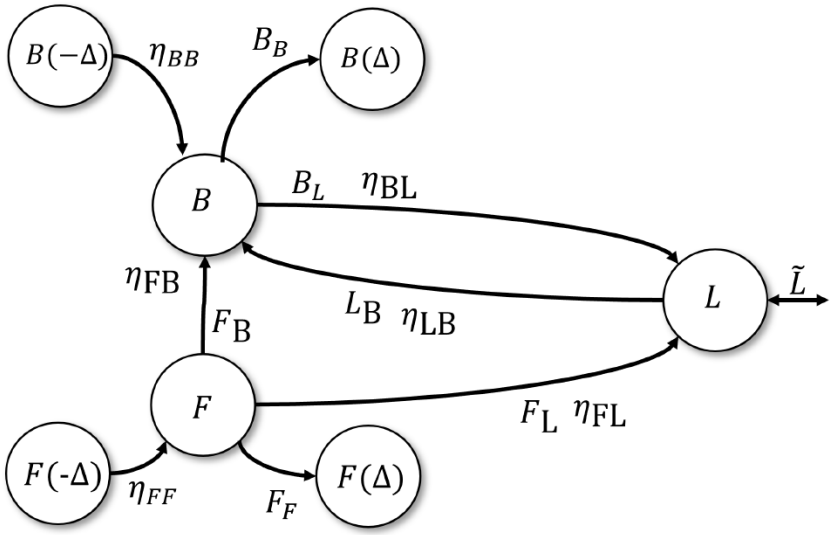

Figure 3-1 : Power flow diagram of a hybrid fuel cell truck with a battery as intermediate storage.

The system is described via flow equations that result from the conservation of energy or the technical requirements. The descriptive system of equations then reads:

$$0 = \eta_{LB} L_B + \eta_{FB} F_B + \eta_{BB} B(-\Delta) - (B_B(\Delta) + B_L)$$

$$0 = \eta_{FF}\, F(-\Delta) - (F_F(\Delta) F_B + F_L)$$

$$\tilde{L} = \eta_{BL} B_L + \eta_{FL} F_L - L_B$$

The first equation describes the power flows to and from the lithium-ion battery. The second equation describes the power flows of the fuel cell and the third equation describes the power flow to and from the load.

In addition to the flow equations, further boundary conditions must be added. Firstly, the total power of the fuel cell is limited to $F_{\max}$ is limited. The sum of the power transferred to the battery F_B and the power transmitted to the load F_L must therefore be less than the maximum power $F_{\max}$

$$F_B + F_L \leq F_{\max}$$

The drive power is also limited to $L_{\max}$ limited. The battery and fuel cell together cannot provide more than this power. We do not consider the power transmitted by the fuel cell and the battery, but only that power which "arrives" at the load after deduction of losses.

$$\eta_{FL} F_L + \eta_{BL} B_L \leq L_{\max}$$

Furthermore, the maximum charging power of the battery $B_{\max}^{\text{charge}}$ must not be exceeded.

$$\eta_{FB} F_B + \eta_{LB} L_B \leq B_{\max}^{\text{charge}}$$

Here, too, the amount of transmitted power is corrected by the transmission losses.

We want to limit the power fluctuations that affect the fuel cell. We represent this by limiting the difference between the discharge power of the previous time -Δ with the discharge power of the current time to $\Delta F_{\max}$:

$$\left|\left(F_B(-\Delta) + F_L(-\Delta)\right) - (F_B + F_L)\right| \leq \Delta F_{\max}$$

By limiting the change in the fuel cell's output, the battery always providing needs to enough power. Therefore, it must be ensured that the state of charge of the battery does not fall below a certain threshold. We express this by the following relation:

$$B_B \geq \frac{\kappa}{\Delta t}\, c_B$$

Where $c_B \in [0,1]$ describes the proportion of the storage capacity that should at least be present.

The equations described so far represent a system of inequalities. We can consider such a system as an optimisation problem. To solve this, we need an objective function, i.e. a measure that allows us to distinguish a good solution from a bad solution. In our case, we focus on the task of minimising losses.

$$\min Y : \left(1 - \eta_{BL}(B_L)\right)B_L + (1 - \eta_{LB}(L_B))L_B + (1 - \eta_{FB}(F_B))F_B + (1 - \eta_{FL}(F_L))F_L$$

In the definition of Y we have not taken into account the losses due to self-discharge. For both storage media, these are low in relation to length of the investigated time series of one working day.

With these equations, the power flows of the system are described. The next step is to determine the system configuration. We have to determine which boundary conditions result from the technology.

4. System configuration

The power flow diagram describes how power is transferred from one component to the next. The technological implementation is reflected so far in the range of values of this power transfer. But the efficiency is also influenced by the choice of power electronic components. We describe this via the transfer losses. If we want a transfer from A to B, i.e. A_B, only the power quantity A'_B arrives:

$$A'_B = A_B - (a_{AB} + b_{AB}A_B + c_{AB}A_B^2)$$

a_{AB}, b_{AB}, c_{AB} are loss coefficients determined by the respective technological realisation. The efficiency results in:

$$\eta_{AB} = \frac{A_B - A'_B}{A_B} = 1 - \left(\frac{a_{AB}}{A_B} + b_{AB} + c_{AB}A_B\right)$$

The advantage of this description is that the loss coefficients are easily accessible experimentally. In our investigation we follow a different approach. To determine the coefficients, we fix the efficiency at three points:

1. Where is the maximum efficiency?
2. What is the maximum efficiency?
3. What is the efficiency at maximum power?

In Table 1 these specifications are given for the various power electronic components. We always relate these data to the maximum power of the components, i.e. we assume that the efficiency curve scales according to the maximum power. The efficiency curves of the four power electronic components resulting from this approach are shown in Figure 4-1.

Table 1 : Definition of the efficiencies of the power electronic components of the FCT

Component	$\eta(P_{max})$	P_{opt}	$\eta(P_{opt})$
Drive	75%	40% P_{max}	85%
Drive inverter	98%	25% P_{max}	95%
Battery Converter	94%	35% P_{max}	92%
Fuel Cell (incl. Converter)	80%	40% P_{max}	85%

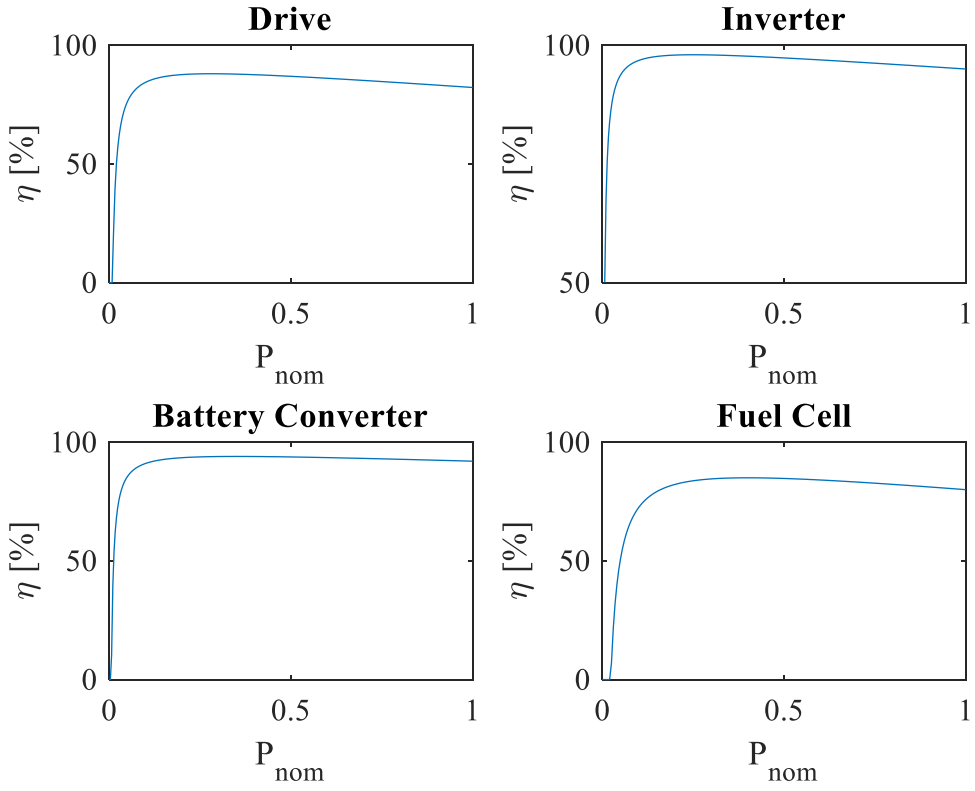

Figure 4-1 : Efficiencies used for the individual components. In the case of the fuel cell, the losses of the fuel cell and fuel cell converter were considered together.

The efficiencies of the power electronic components do not yet correspond to the efficiencies of the power transfer from one node to another. For this, the different stages must be considered in combination. For example, in the case of a power transfer from the fuel cell to the drive, the losses of the fuel cell converter, then of the drive inverter and then of the motor must first be determined. These different steps can then be combined into an efficiency curve. In Figure 4-2 the efficiency curves for battery and fuel cell to load are shown. The resulting efficiency for a power transfer is lower than the efficiency of the individual component.

This is to be expected, so in a power transfer from the fuel cell to the battery, the power would first be transferred through the fuel cell, then through the fuel cell converter and the battery converter. All three components reduce the overall efficiency through their losses.

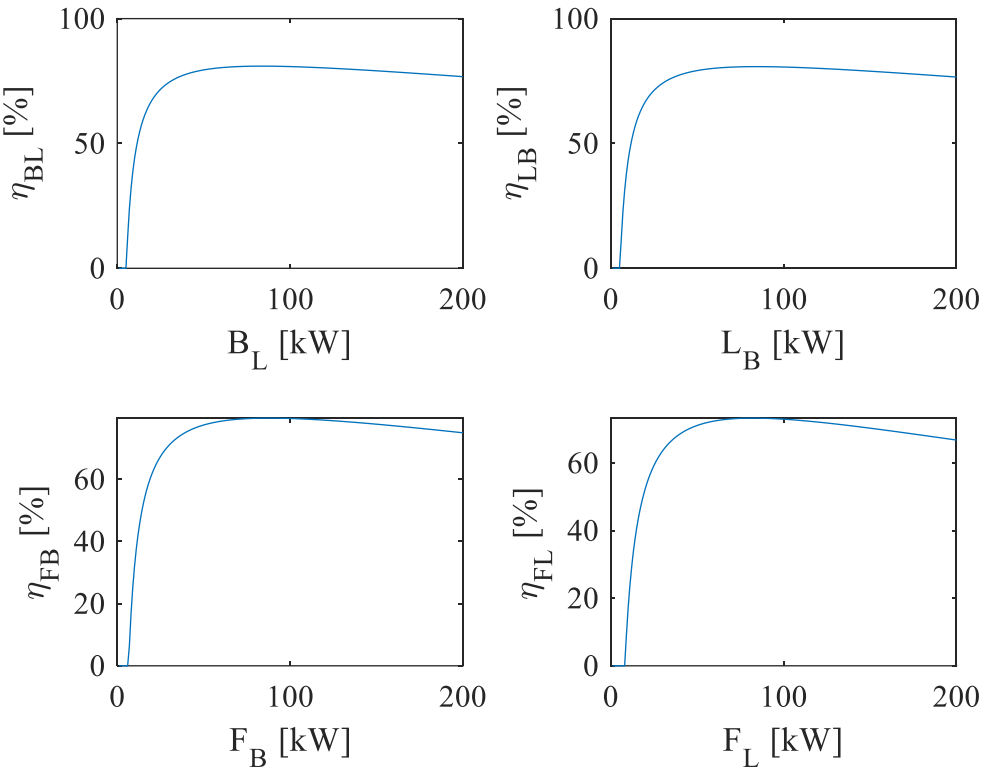

Figure 4-2 : Efficiency curves of the four power transfers between the fuel cell, the battery, and the power supply. F the battery B and the load L.

5. Power flow of a commercial vehicle

For the design and the evaluation of different configurations we need a load profile $\tilde{L}$. The load profile represents the power demand over time. We assume that there is no interaction between the power supply and the power demand, i.e. we do not close the control loop. This is a simplification, because the driver would adapt his driving behaviour to the power supply of the fuel cell and battery. If a certain peak power were demanded that could not be provided, the vehicle would accelerate longer or the driver would abort an overtaking manoeuvre. These interactions are not considered here. The aim of using the power flow diagram is to quantitatively compare different technical approaches with relatively little effort.

In this study, we consider the performance profile of a long-haul transporter [8][14]. In Figure 5-1 the load profile and its histogram are shown. The load profile is characterised by sections with a longer journey and a phase of smaller journeys and idle times. In our analysis, we want to assume that there is no external charging possibility during this time, i.e. the vehicle must have charged its energy at the beginning of the journey.

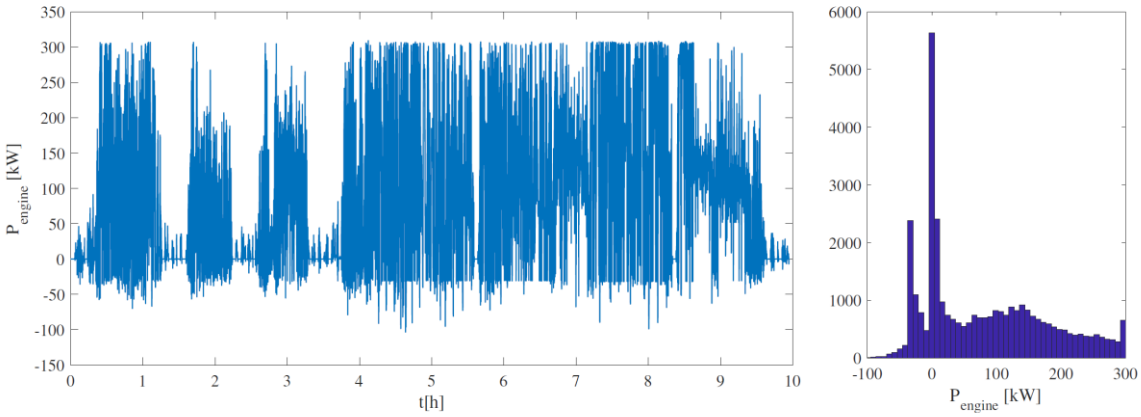

Figure 5-1 : Load profile of the hybrid fuel cell truck [8]

The system consideration is now carried out as follows: First, a system configuration is defined. Then the optimisation problem is solved at each point in time, i.e. at each point in time it is looked at which power flows can minimise the losses and still provide the required power flow. In Figure 5-2 an exemplary solution is shown. The power flows are sometimes higher than the load. This is because the transfer losses must be taken into account. If a power P is required by the drive, power must be $\frac{P}{\eta}$ be transferred.

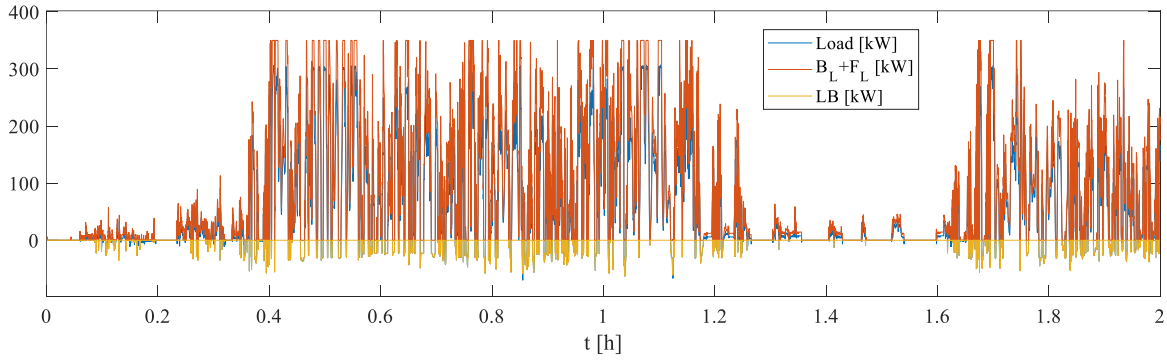

Figure 5-2 : Load profile (Load) and load flows of an example configuration.

6. System design

The question of how the fuel cell is used depends on the question of how high the permitted power gradients are that are to be allowed to the fuel cell. Let us first consider the case of a small maximum power gradient of $\Delta F_{\max} = 0{,}05\,\frac{\mathrm{kW}}{\mathrm{s}}$. Here, the goal would be to operate the fuel cell as permanently as possible. Therefore $c_B = 50\%$ is selected, i.e. as soon as the battery capacity falls below 50%, the fuel cell begins to charge. In Figure 6-1 (left) it can be clearly seen how the discharge of the fuel cell slowly increases. However, this increase is not fast enough, so that the battery is completely discharged for a short moment. This effect cannot be observed with the large gradient (Figure 6-1 (right)). The fuel cell starts its final charge very early, but does not charge the battery either, as its state of charge is still above the threshold.

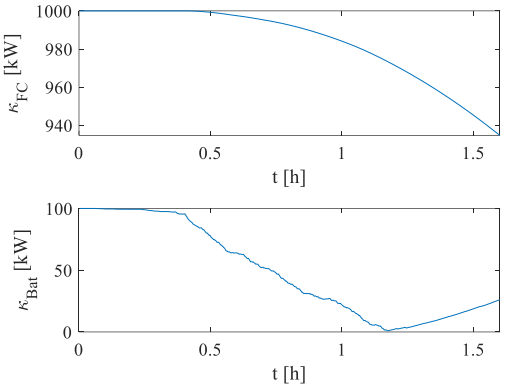

$\Delta F_{max} = 0{,}05 \frac{kW}{s}$.

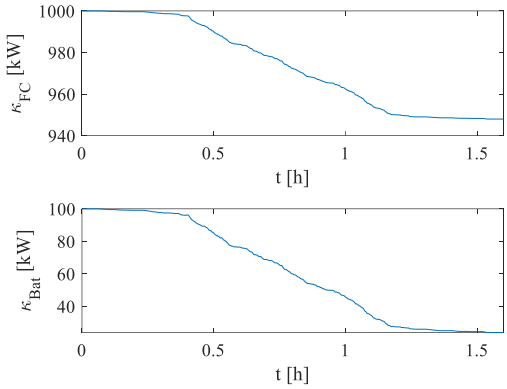

$\Delta F_{max} = 100 \frac{kW}{s}$

Figure 6-1 : Capacity curve with a small gradient of $\Delta F_{max} = 0{,}05 \frac{kW}{s}$ and a large gradient of $\Delta F_{max} = 100 \frac{kW}{s}$ are shown. The threshold for charging the battery is 50% for the small gradient and 5% for the large gradient.

The power flows of these two configurations are also different. In Figure 6-2 the power flows of both configurations are shown. As the capacity curve of the fuel cell suggests with a small gradient, the power flow increases linearly. There is a small area where the power from the fuel cell is also used to cover the load, but most of the power here flows into the battery.

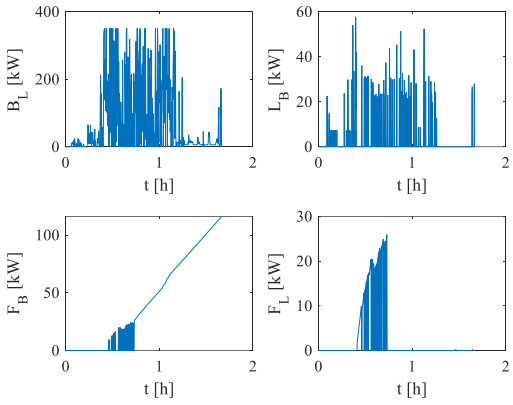

$\Delta F_{max} = 0{,}05 \frac{kW}{s}$.

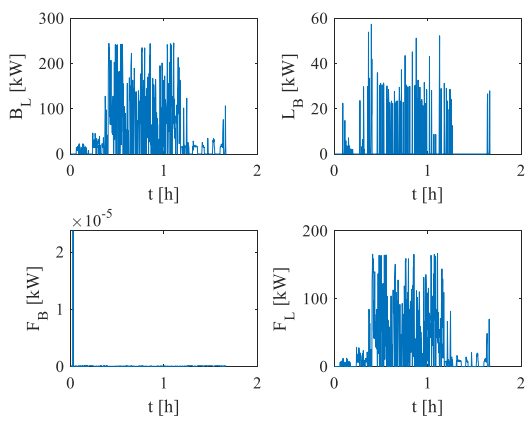

$\Delta F_{max} = 100 \frac{kW}{s}$

Figure 6-2 : Power flows for a drivetrain with a small gradient and a large gradient. The threshold for charging the battery is 50% for the small gradient and 5% for the large gradient.

With a large gradient, we see that no power is transferred to the battery. Instead, the fuel cell is used together with the battery to cover the load. Since charging the battery causes higher losses than if the load were covered directly, this division makes sense.

In Figure 6-1 and Figure 6-2 we have used a short section of the load profile from Figure 5-1. We now want to try to determine an optimal configuration with the help of suitable measured variables. In doing so, we consider four variables that are derived from four requirements.

We want to ensure that the load is always supplied, with the help of the Missing Load Ratio M we describe the proportion of the power points in the load profile $\tilde{L}$ that are not covered in the time run:

$$M = \frac{\tilde{L} - (\eta_{FL} F_L + \eta_{BL} B_L)}{\tilde{L}}$$

In our simulation, we have no feedback between the driver and the load profile, i.e. a shortfall in the load has no effect on the further driving process. This simplifies the computational effort so that the results are nevertheless meaningful, should M not be too large.

Furthermore, we consider the overall efficiency η of the power flow since the objective function Y has the objective of avoiding the losses.

$$\eta = 1 - \frac{\sum_{t=0}^{t=T_{\text{end}}} Y}{\sum_{t=0}^{t=T_{\text{end}}} B_L + L_B + F_B + F_L}$$

To extend the service life of the fuel cell, we have introduced the limitation of the power gradient. As a further measure we consider the mean power gradient ΔF_{rms}. This indicates which gradient is observed on average for the entire journey.

$$\Delta F_{\text{rms}} = \frac{1}{T_{\text{end}}} \sqrt{\sum_{t=0}^{t=T_{\text{end}}} (\Delta F)^2}$$

The last key figure is the total energy consumption κrequired to drive through the load profile. We assume that the hydrogen tank is very large. The vehicle always carries enough energy to finish its tour. We can therefore determine the consumption from the filling quantity that remains in the tank at the end.

In the following we consider the influence of ΔF_{max} on these four variables. Here we work with a battery capacity of $100\ \text{kWh}$. Unlike in [9] we do not limit the charging and discharging capacities here. This means that the lithium-ion battery can be used with a maximum discharge power of 4C. Which is possible for shorter times with modern cells.

We vary ΔF_{max} over a range of values from $0{,}01\,\frac{\text{kW}}{\text{s}}$ to $10\,\frac{\text{kW}}{\text{s}}$ and consider the described quantities. In Figure 6-3 the result of this experiment is shown. Due to the large range of values, we choose a logarithmic x-axis.

The Missing Load Ration M shows that even with a very small value for ΔF_{max} only 1-1.5% of the load values are not fulfilled. Since we work with a very large hydrogen tank, these losses are only due to the inertia of the fuel cell. That is, to those cases where the fuel cell does not yet contribute enough power. This "inertia effect" lasts up to a value of approx. $1\,\frac{\text{kW}}{\text{s}}$. From then on M drops.

The efficiency η varies over the entire value range of the experiment between 74% and 75.5%. The drop from approx. $0{,}4\,\frac{\text{kW}}{\text{s}}$. In this range the fuel cell works much better as a range extender, as we know from the observations on M i.e. the power fed in corresponds better to the demand of the battery than in a sluggish setting. The consequence of this is that the power provided by the fuel cell is transferred to the battery via an additional conversion stage, which reduces the overall efficiency. If we reduce the inertia of the fuel cell by ΔF_{max} increasing it further, a transition occurs in which the fuel cell no longer serves as a range extender but as a power source for the load. In this case, the power provided by the fuel cell is used more efficiently, which we can observe through the increase in observed efficiency.

The increase in efficiency is also noticeable in the κ. With a sluggish fuel cell, consumption is higher with $1400\ \text{kWh}$ compared to a configuration with a high ΔF_{max} 16% higher. At a value of $\Delta F_{\text{max}} \approx 2\,\frac{\text{kW}}{\text{s}}$ this reaches its maximum. Surprisingly, the consumption increases again at an even higher value.

This is because the fuel cell's share in supplying the load then also increases and the fuel cell's losses rise as a result.

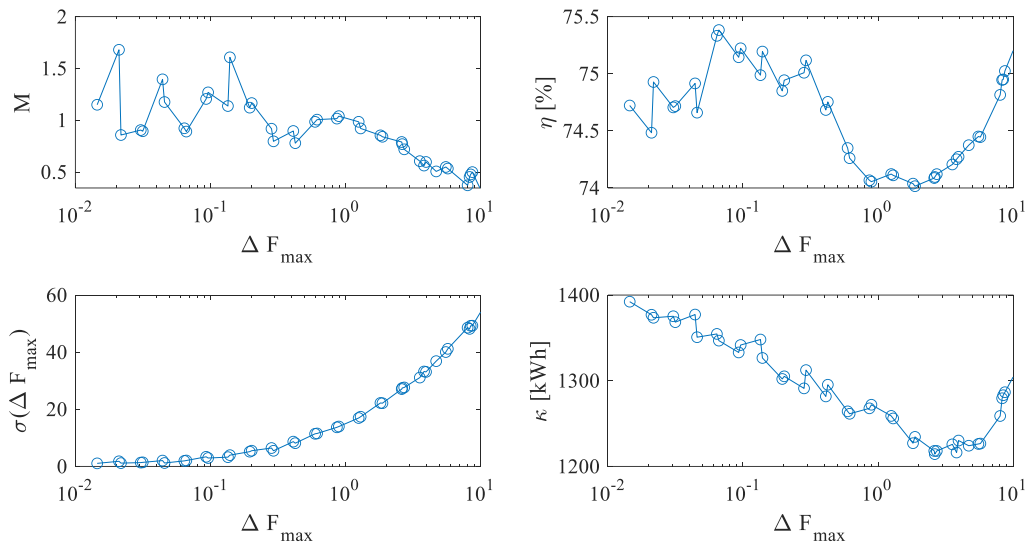

Figure 6-3 : Evaluation of the trips with different maximum gradients $\Delta F_{\max}$ with a battery capacity of 100 kWh.

These experiments show that for the load profile considered here, a gradient of $\Delta F_{\max} = 2\,\frac{\mathrm{kW}}{\mathrm{s}}$ is optimal for the efficiency of the system.

7. Conclusion

Mobile machines and commercial vehicles are technically demanding, complex energy storage systems whose design involves the analysis of different issues. For a quick analysis of different technical realisations, the power flow diagram can be a simple help. In this paper, we considered the method for the design of a truck with a hybrid drive system consisting of battery and fuel cell. The focus here was on the question of what limitation of the power gradient must be worked with and what effect its limitation has on different key figures. Regarding energy consumption, it was shown that we can reduce consumption by 15% if we allow a power gradient of $\Delta F_{\max} = 2\,\frac{\mathrm{kW}}{\mathrm{s}}$. The reason for this is that the use of the fuel cell as a range extender generates additional losses due to the additional conversion stage.

The method chosen here allows further analyses that may be relevant for the design. For example, we did not vary the properties of the power electronics here and did not consider the effect of different circuit topologies or the evaluation of different battery cell technologies. Also, the optimisation problem was only solved at one time point and not over a longer time range. This would allow additional insights into the performance of the best possible operation management.

Nevertheless, this study was able to show how an initial quantitative assessment of the optimal design can be realised with simple, experimentally accessible data and parameters.

References

[1] A. Lajunen, P. Sainio, L. Laurila, J. Pippuri-Mäkeläinen, and K. Tammi, "Overview of powertrain electrification and future scenarios for non-road mobile machinery," *Energies (Basel),* vol. 11, no. 5, 2018, doi: 10.3390/en11051184.

[2] M. Liukkonen, A. Lajunen, and J. Suomela, "Feasibility study of fuel cell-hybrid powertrains in non-road mobile machineries," *Autom Constr*, vol. 35, pp. 296-305, 2013, doi: 10.1016/j.autcon.2013.05.019.

[3] K. Tammi, P. Sainio, and D. Student, "Hybrid and electric Non-Road Mobile Machines (NRMM) For further interest on NRMM roadmap," 2017.

[4] Armin U. Schmiegel, "The Straddle Carrier as an example for the electrification of mobile machines," Reutlingen, 2022.

[5] J. Kukkaro, "Straddle Carrier Electric Powertrain Optimization," no. August, 2016.

[6] P. Garcia, L. M. Fernandez, C. A. Garcia, and F. Jurado, "Fuel Cell-Battery Hybrid System for Transport Applications," no. November, 2009, doi: 10.1109/ICEMS.2009.5382685.

[7] Md. R. Habib *et al.* , *Recent Progress in Energy Management System for Fuel Cell Hybrid Electric Vehicle*, no. February 2022. Springer Singapore, 2022. doi: 10.1007/978-981-16-4321-7_60.

[8] A. U. Schmiegel, *Energy Storage Systems,* vol. in Press. Oxfort: Oxfort University Press, 2022.

[9] Armin U. Schmiegel, "From the smoking exhaust to the clean socket Design steps from the diesel-powered mobile machine to the all-electric mobile machine Part 1 - Power and Energyconsiderations," Reutlingen, 2022.

[10] A. U. Schmiegel and A. Kleine, "Upper economical performance limits for pv storage systems," in *28th European Photovoltaic Solar Energy Conference*, 2013, pp. 1-20.

[11] A. Kleine and A. U. Schmiegel, "Optimized Operation strategies for PV Storages systems - Yield limitations, optimized battery configuration and the benefit of a perfect forecast," *Energy Procedia*, vol. 46, pp. 104-113, 2014, [Online]. Available: http://dx.doi.org/10.1016/j.egypro.2014.01.163

[12] P. Pei and H. Chen, "Main factors affecting the lifetime of Proton Exchange Membrane fuel cells in vehicle applications: A review," *Appl Energy*, vol. 125, pp. 60-75, 2014, doi: 10.1016/j.apenergy.2014.03.048.

[13] F. B. Weng, C. Y. Hsu, and C. W. Li, "Experimental investigation of PEM fuel cell aging under current cycling using segmented fuel cell," *Int J Hydrogen Energy*, vol. 35, no. 8, pp. 3664-3675, 2010, doi: 10.1016/j.ijhydene.2010.01.065.

[14] N. R. E. Laboratory, "NREL DriveCAT - Chassis Dynamometer Drive Cycles," 2022. http://www.nrel.gov/transportation/drive-cycle-tool (accessed May 01, 2022).